Am J Physiol Endocrinol Metab 296: E1354–E1362, 2009.
First published March 17, 2009; doi:10.1152/ajpendo.90836.2008.

Role for malic enzyme, pyruvate carboxylation, and mitochondrial malate import in glucose-stimulated insulin secretion

Emma Heart,[1] Gary W. Cline,[2]* Leon P. Collis,[1]* Rebecca L. Pongratz,[2] Joshua P. Gray,[3] and Peter J. S. Smith[1]

[1]*BioCurrents Research Center, Molecular Physiology Program, Marine Biological Laboratory, Woods Hole, Massachusetts;* [2]*Department of Internal Medicine, Yale University School of Medicine, New Haven; and* [3]*US Coast Guard Academy, New London, Connecticut*

Submitted 13 October 2008; accepted in final form 12 March 2009

Heart E, Cline GW, Collis LP, Pongratz RL, Gray JP, Smith PJS. Role for malic enzyme, pyruvate carboxylation, and mitochondrial malate import in glucose-stimulated insulin secretion. *Am J Physiol Endocrinol Metab* 296: E1354–E1362, 2009. First published March 17, 2009; doi:10.1152/ajpendo.90836.2008.—Pyruvate cycling has been implicated in glucose-stimulated insulin secretion (GSIS) from pancreatic β-cells. The operation of some pyruvate cycling pathways is proposed to necessitate malate export from the mitochondria and $NADP^+$-dependent decarboxylation of malate to pyruvate by cytosolic malic enzyme (ME1). Evidence in favor of and against a role of ME1 in GSIS has been presented by others using small interfering RNA-mediated suppression of ME1. ME1 was also proposed to account for methyl succinate-stimulated insulin secretion (MSSIS), which has been hypothesized to occur via succinate entry into the mitochondria in exchange for malate and subsequent malate conversion to pyruvate. In contrast to rat, mouse β-cells lack ME1 activity, which was suggested to explain their lack of MSSIS. However, this hypothesis was not tested. In this report, we demonstrate that although adenoviral-mediated overexpression of ME1 greatly augments GSIS in rat insulinoma INS-1 832/13 cells, it does not restore MSSIS, nor does it significantly affect GSIS in mouse islets. The increase in GSIS following ME1 overexpression in INS-1 832/13 cells did not alter the ATP-to-ADP ratio but was accompanied by increases in malate and citrate levels. Increased malate and citrate levels were also observed after INS-1 832/13 cells were treated with the malate-permeable analog dimethyl malate. These data suggest that although ME1 overexpression augments anaplerosis and GSIS in INS-1 832/13 cells, it is not likely involved in MSSIS and GSIS in pancreatic islets.

dimethyl malate; pyrurate cycling; methyl succinate; anaplerosis

INSULIN SECRETION FROM PANCREATIC β-cells is dependent on the metabolism of secretory fuels. Apart from oxidative pathways leading to the rise in the ATP-to-ADP ratio and resulting in the ATP-dependent K^+ (K_{ATP}) channel-dependent sequence of events (18, 34), it has been proposed that efflux of tricarboxylic acid (TCA) cycle intermediates out of the mitochondria (9, 26, 28) leads to the synthesis of other coupling factors, which couple β-cell metabolism with insulin secretion. Candidates for these coupling factors include NADPH, short-chain acyl-CoAs, glutamate, long-chain acyl-CoAs, and malonyl-CoA, (20, 26, 31, 32, 40); however, evidence against malonyl-CoA and glutamate has been presented (1, 29, 36).

The efflux of TCA cycle intermediates is contingent on the anaplerotic influx of pyruvate into the TCA cycle. Conversion of these TCA cycle intermediates back to pyruvate in the cytosol occurs via pyruvate cycling pathways. Pyruvate cycling has been implicated as an important component of glucose-mediated insulin secretion. According to the proposed model, pyruvate cycling can occur via the action of $NADP^+$-dependent cytosolic malic enzyme (ME1), which enables the pyruvate-malate (26) and pyruvate-citrate (9) pathways. It can also take place via the action of cytosolic isocitrate dehydrogenase (ICDc), which enables the pyruvate-isocitrate pathway (41). In the malate-pyruvate pathway, malate is exported from the mitochondria to the cytosol and converted directly to pyruvate by ME1. In the pyruvate-citrate pathway, citrate is exported from the mitochondria to the cytosol, where malate is produced via aconitase, citrate lyase, and malate dehydrogenase reactions and then converted by ME1 to pyruvate. In the pyruvate-isocitrate pathway, isocitrate is exported from the mitochondria to the cytosol and can be oxidized by ICDc to α-ketoglutarate (α-KG), which then can enter mitochondria and be converted to malate via TCA cycle reactions.

A series of reports support the role of pyruvate cycling in glucose-stimulated insulin secretion (GSIS) by demonstrating that the level of GSIS correlates with an increase in pyruvate cycling (24), whereas inhibition of the pyruvate-isocitrate shuttle, via inhibition of the ICDc or the citrate-isocitrate carrier, impairs GSIS (21, 41). Inhibition of the pyruvate-malate and pyruvate-citrate shuttles, via inhibition of ME1, also impairs GSIS (13, 39), whereas potentiation of GSIS by the membrane-permeable malate analog dimethyl malate (DMM) has been proposed to take place via activation of pyruvate cycling (5). However, the role of ME1 in GSIS has been disputed in a recent report in which small interfering RNA-mediated inhibition of ME1 did not affect GSIS in rat islets (42).

Although all three pathways are operative in rat β-cells, only the isocitrate pathway operates in mouse β-cells, likely because of the absence or relatively low level of $NADP^+$-dependent malic enzyme activity (2, 17, 27). Absence of the malate-pyruvate cycle in mouse islets was suggested to account for their weak second phase of GSIS (39) and their inability to secrete insulin in response to methyl succinate (MS), a membrane-permeable succinate analog (27). It has been suggested that MS-stimulated insulin secretion (MSSIS) is contingent on the presence of ME1 activity (27), in such a way that succinate import into the mitochondria is balanced by export of malate and subsequent conversion of malate to pyruvate via ME1 in the cytosol. However, this hypothesis has not been tested.

This study was undertaken to determine the mechanism by which ME1 activity enhances insulin secretion and to test the hypothesis that the response to MS is contingent on the

* G. W. Cline and L. P. Collis contributed equally to this work.

Address for reprint requests and other correspondence: E. Heart, BioCurrents Research Center, Marine Biological Laboratory, 7 MBL St., Lillie 219, Woods Hole, MA 02543 (e-mail: eheart@mbl.edu).

presence of ME1 (27). Our data demonstrate that overexpression of ME1 potentiates GSIS in rat insulinoma INS-1 832/13 cells and that this effect is accompanied by an increase in mitochondrial malate and citrate levels, whereas the ATP-to-ADP ratio was not affected. However, introduction of ME1 activity into mouse pancreatic β-cells did not significantly augment GSIS, nor did it restore the secretory response to MS, as previously hypothesized (27). These data suggest that although ME1 regulates metabolism and GSIS in INS-1 832/13 cells, it is not directly involved in MSSIS or GSIS in islets.

MATERIALS AND METHODS

Cell preparation and culture. Clonal INS-1 832/13 cells and MIN-6 cells were provided by Drs. Christopher Newgard (Duke University) and Jun-ichi Miyazaki (Osaka University) and were maintained and cultured as described previously (19, 35). Male CD-1 mice (Charles River) were euthanized by halothane. All procedures were performed in accordance with the Institutional Guidelines for Animal Care in compliance with US Public Health Service regulations and were approved by the Institutional Animal Care and Use Committee (IACUC no. 08-36) at the Marine Biological Laboratory. Pancreatic islets were isolated by collagenase (Roche, Indianapolis, IN) digestion (16). Islets were used immediately after isolation for viral transduction or after an overnight culture in RPMI supplemented with 10% fetal calf serum (Hyclone), penicillin-streptomycin, and 5 mM glucose and were dispersed by incubation in Ca^{2+}/Mg^{2+}-free PBS, 3 mM EGTA, and 0.002% trypsin, as described elsewhere (16). Islet cells were plated on poly-D-lysine-coated coverslips (MatTek, Ashland, MA) in 35-mm petri dishes (for Ca^{2+} studies and immunocytochemistry). INS-1 832/13 cells (at 60–70% confluency), single mouse islet cells, and whole mouse islets were transduced with Ad-ME1-GFP or Ad-CV-GFP at 50 multiplicity of infection for 12 h; then viral medium was replaced with appropriate growth medium. Insulin secretion and Ca^{2+} responses were determined 48 h after transduction. Transduction efficiency in single cells, determined from green fluorescent protein (GFP) fluorescence, reached >90% under these conditions. Islets and single cells were used 48 h after transduction. ME1 expression was monitored by GFP fluorescence and measurement of ME1 mRNA and protein level, as well as ME1 enzymatic activity.

Purification of ME1. INS-1 832/13 cells, at 80% confluency, were fractionated using a cytosol fractionation kit (Calbiochem) according to the manufacturer's protocol. Cytosolic fractions were further purified by NADPH affinity chromatography using the substrate activation method (47, 49). Briefly, 2′,5′-ADP-agarose was added (0.2 ml volume of settled resin per volume of cytosol), and the suspension was rocked for 1 h at 4°C and then centrifuged at 2,000 *g* for 5 min. The supernatant was discarded, and the resin was washed five times with PBS. For elution of ME1, the resin was washed with PBS containing 0.1% NP-40 and 5 mM NADPH (12). For removal of NADPH from the eluate, the eluate was first concentrated using a centrifugal filter (Amicon Ultra 50, Millipore, Billerica, MA). Retentate was reconstituted to the original volume with PBS, and this process was repeated six times. Under these conditions, the concentration of NADPH in the sample was <10 nM, as determined spectrophotometrically.

Malic enzyme activity. For determination of the rate of reductive decarboxylation of malate, protein extracts (20 μg) or NADPH standard (1–100 nmol) was added to the reaction buffer [50 mM HEPES (pH 7.4), 5 mM $MnCl_2$, 50 μM $NADP^+$, and 10 mM malate] in a cuvette positioned inside a temperature-controlled chamber maintained at 37°C. The cuvette content was stirred to ensure proper mixing. Fluorescence was measured at 340-nm excitation and 460-nm emission on a fluorescence spectrophotometer (FluoroMax-3, Horiba Jobin Yvon). A calibration curve was generated using known amounts of NADPH (the product of malate reductive decarboxylation) in the reaction buffer (17). For determination of the rate of NADPH oxidation via oxidative carboxylation of pyruvate, protein extracts (20 μg) were added to the reaction buffer containing 50 mM HEPES (pH 7.4), 50 μM NADPH, 10 mM pyruvate, 30 mM $NaHCO_3$, and 5 mM $MnCl_2$. To correct for the chemical instability of NADPH, the rate of enzymatic oxidation of NADPH was calculated as the difference between the rates of total NADPH oxidation and nonenzymatic NADPH oxidation, which were determined in the presence of enzyme source and vehicle (PBS), respectively.

Construction of adenoviruses. Recombinant, replication-deficient type 5 adenoviruses expressing cytosolic firefly luciferase (Ad-CytoLuc) or human ME1 from OriGene (Ad-ME1-GFP) were directly purchased from (Ad-CytoLuc) or custom-constructed (Ad-ME1-GFP) by Vector BioLabs (Philadelphia, PA). The expression of ME1 is under the control of cytomegalovirus, which also directs the transcription of GFP from an internal ribosome entry site. A control virus (Ad-CV-GFP) was constructed in parallel. Viral titers were determined by the plaque formation assay.

Immunocytochemistry. At 48 h after transduction, cells were washed twice with PBS and fixed with 4% paraformaldehyde. Cells were permeabilized in 0.1% Triton X-100 for 15 min and probed with an mouse anti-human ME1 antibody (1:500 dilution; Abnova) and rabbit anti-mouse insulin antibody (1:200 dilution; Immunostar) in 10% normal goat serum blocking solution for 1 h (Zymed Labs). A negative control contained only blocking serum. The primary antibodies were probed with Alexa Fluor 546 goat anti-mouse IgG and Alexa Fluor 647 goat anti-rabbit IgG (1:1,000 dilution; Invitrogen) for 1 h. Cells were costained with the nuclear DNA marker 4′,6-diamidino-2-phenylindole (DAPI, 300 nM; Invitrogen) before they were imaged using a laser scanning confocal microscope (LSM 510 Meta, Zeiss) with a ×63 oil immersion objective (1.4 NA, ~0.7 μm *z*-resolution). Fluorescence images of *x-y* sections were recorded with 512 pixels per line. Raster point size was 60 nm, with an overall lateral resolution of 0.2 μm. GFP, Alexa Fluor 546, and Alexa Fluor 647 were excited at the 488-, 543-, and 633-nm laser lines, respectively, with emission collected through a 488/543/633-nm dichroic mirror. DAPI was imaged with two-photon excitation (Ultrafast Ti: Sapphire, Coherent) tuned to 720 nm, and emission was collected through a 700/488-nm dichroic mirror. Digital image overlay was performed using Adobe Photoshop (version 6, Adobe Systems).

Ca^{2+} measurement. Cells were loaded for 60 min with the Ca^{2+} indicator Fura Red-AM (Molecular Probes, Eugene, OR) in the presence of 0.2% Pluronic F127 in the growth medium. Cells were washed in Krebs-Ringer bicarbonate [KRB; 5 mM glucose, 140 mM NaCl, 30 mM HEPES, 4.6. mM KCl, 1 mM $MgSO_4$, 0.15 mM Na_2HPO_4, 0.4 mM KH_2PO_4, 5 mM $NaHCO_3$, 2 mM $CaCl_2$, and 0.05% BSA (pH 7.4)] and imaged on a laser scanning confocal microscope (LSM 510 Meta) equipped with a heated stage. Fura Red was excited using a 488-nm argon laser line, and emitted light was collected with a 650-nm long-pass filter. At these settings, no contamination from GFP was detected. Images were analyzed by the LSM Image Browser software to derive Ca^{2+} profiles. After the experiment, confocal dishes were fixed with 4% paraformaldehyde, and β-cells were identified using rabbit anti-mouse insulin antibody (1:200 dilution; Immunostar) probed with Alexa Fluor 647 goat anti-rabbit IgG (1:1,000, Invitrogen). Only insulin-positive cells were included in the analysis.

ATP levels. Changes in cytosolic ATP concentration were measured after cell infection with adenovirus carrying cytosolically targeted luciferase (Ad-CytoLuc) using the luciferin-luciferase reaction (33). Coverslips with cells, mounted inside a 35-mm dish (MatTek) were placed directly onto the surface of the photocathode optical window of a photomultiplier tube (model R464; Hamamatsu) housed in a 37°C heated box. After application of 100 μM luciferin, the signal was allowed to reach a steady-state level, and changes in the concentration of ATP in response to fuel addition were determined by measurement of luminescence.

O_2 consumption. O_2 consumption in single islets in response to fuel additions was measured by the self-referencing method based on an electrochemical O_2 sensor moving between the "near" and "far" position from the islet (48). The magnitude of the amperometric current used for the reduction of O_2 is proportional to the O_2 concentration at that particular point.

Insulin secretion. Cells were preincubated for 2 h in the presence of 2 mM (INS-1 832/13 cells) or 4 mM (mouse islets) glucose in KRB buffer. The amount of released insulin was determined after 30 min of static incubation in the presence of secretory fuels using a radioimmunoassay kit (Linco Research, St. Charles, MO) with rat insulin as the standard. Data were normalized for protein content determined by a micro-bicinchoninic acid protein assay kit (Pierce, Rockford, IL).

Tandem mass spectrometry analysis of metabolites. After 30 min of incubation, cells were collected by centrifugation or subjected to rapid fractionation to obtain mitochondria with use of a fractionation kit (BioVision, Mountain View, CA). The pellets were suspended in 200 μl of ice-cold acetonitrile-water (1:1) with 2 mM ammonium acetate and 10 μM [1,2-$^2H_2$]taurine (d4-taurine), disrupted by sonication, and centrifuged. The supernatant was analyzed by tandem mass spectrometry (LC-MS/MS). Metabolite levels were calculated from standard curves, with d4-taurine as the internal standard, and normalized to DNA concentration. LC-MS/MS analysis of metabolites was performed on an Applied Biosystems API4000 QTrap interfaced to a Shimadzu HPLC (LC-20AD, SIL-20AC, CTO-20A). Metabolites were eluted from a 5-μm, 120-Å, 4.5 × 250 mm C_{16} column (Dionex Aclaim Polar Advantage) at 40°C with acetonitrile-water buffered with 2 mM ammonium acetate using a linear gradient from 5% to 95% acetonitrile at a flow rate of 600 μl/min. Metabolite concentrations were determined by electrospray ionization monitoring of the positive-product ion transition pairs of ATP (506.0/158.9), ADP (426.0/158.9), citrate (191.0/87.0), malate (133.0/71.0), and d4-taurine (127.9/80.0).

Glucose oxidation. Groups of 30 islets or 2.5 × 10^5 INS-1 832/13 cells were incubated in a 0.6-ml Eppendorf tube without a cap in the presence of 2 or 10 mM glucose and D-[U-^{14}C]glucose (PerkinElmer; 250 mCi/mmol). The Eppendorf tube was placed upright in an airtight sealed 20-ml scintillation vial, which contained an empty 1.5-ml Eppendorf tube without a cap. After 90 min of incubation at 37°C with agitation, the reaction was terminated by the injection of 10 μM rotenone, 10 μM antimycin, and 1 mg KCN. The 1.5-ml tube was emptied in the scintillation vial by injection of 500 μl of 5% KOH. After 60 min of incubation at room temperature, glucose oxidation was determined by measurement of the KOH-trapped $^{14}CO_2$.

Statistical analysis. Values are means ± SE. Significance was determined for multiple comparisons using one-way ANOVA; $P < 0.05$ was considered significant.

RESULTS

Kinetic characteristics of ME1. To obtain a large uniform supply of highly concentrated enzyme needed for kinetic studies and to avoid possible contamination of the source with other cytosolic enzymes, we purified ME1 from INS-1 832/13 cells. Enzyme activity following individual purification steps is shown in Table 1. Purification resulted in an ~2,000-fold increase in specific activity measured by oxidative carboxylation of pyruvate and reductive decarboxylation of malate. In the final fraction, levels of oxidative carboxylation of pyruvate reached ~85% of the reductive decarboxylation of malate. K_m values determined at pH 7.4 for malate and pyruvate were 240 μM and 5.8 mM, respectively, in agreement with a previous report on ME1 from liver and skeletal muscle (52).

Effect of ME1 overexpression on ME1 activity, GSIS, ATP-to-ADP ratio, and malate and citrate levels. Adenoviral-mediated expression of ME1 cDNA in INS-1 832/13 cells resulted in a significant increase in $NADP^+$-dependent malic enzyme activity (from 8.1 ± 2 to 115 ± 22 μmol NADPH·mg cytosol protein^{-1}·min^{-1}). Similar treatment of mouse islets led to the introduction of protein-soluble $NADP^+$-dependent malic enzyme activity (from nondetectable levels to 123 ± 23 μmol NADPH·mg cytosol protein^{-1}·min^{-1}). Immunocytochemical detection of transduced ME1 protein is shown in Fig. 1. In INS-1 832/13 cells, ME1 overexpression significantly potentiated glucose- and methyl pyruvate (MP)-stimulated, but not MS-stimulated, secretion (Fig. 2*A*). KCl-induced secretion remained unchanged, suggesting that a metabolic, rather than an ionic, mechanism underlies the increase in secretion. The fuel-dependent increase in intracellular ATP level was not changed in ME1-overexpressing cells compared with controls, as determined by measurements from the luciferin-luciferase reaction in populations of INS-1 832/13 cells coexpressing cytosolically targeted luciferase and ME1 or control (Fig. 2*B*). Similarly, neither the ATP-to-ADP ratio nor the rate of glucose oxidation (Table 2) was affected by ME1 overexpression. ME1 overexpression resulted in an increased glucose-dependent rise in malate and citrate levels (Fig. 2, *C* and *D*) in INS-1 832/13 cells. Introduction of ME1 activity altered GSIS to a lesser degree in mouse islets than in INS-1 832/13 cells (Fig. 3*A*). As in INS-1 832/13 cells, ATP levels remained unaffected (Fig. 3*B*).

Table 1. *Purification of ME1 from INS-1 832/13 cells*

Step	Specific Activity, μmol NADPH·min^{-1}·mg protein^{-1}	Purification, fold change
Total homogenate	0.34±0.035	1
Cytosol	10±1.4	29.4
2′,5′-ADP-agarose	758±56 (687±34)*	2,229.4

Values are means ± SE from 3–4 independent experiments. ME1, cytosolic malic enzyme. *Oxidative carboxylation of pyruvate.

Malate is a component of the malate-pyruvate pathway, and its membrane-permeable analog DMM has been proposed to counteract lipid-induced impairment of GSIS by enhancing pyruvate cycling pathways in INS-1 832/13 cells (5). We have confirmed that DMM nearly doubles GSIS in INS-1 832/13 cells (Fig. 2*A*), an effect that is accompanied by an increase in malate and citrate levels (Fig. 2, *C* and *D*). However, we have also demonstrated that DMM nearly doubles GSIS in isolated mouse islets (Fig. 3*A*), where the malate-pyruvate shuttle is not operative because of the absence of ME1. To clarify the mechanism by which DMM potentiates GSIS, we tested the effect of DMM on GSIS in the INS-1 832/13 cells and mouse islets overexpressing ME1. ME1 overexpression removed the potentiating effect of DMM on glucose-mediated secretion in both cell preparations, suggesting that activation of the malate-pyruvate shuttle by malate does not directly underlie the mechanism of DMM action (Figs. 2*A* and 3*A*). In accordance with these findings, mitochondrial malate levels were increased in INS-1 832/13 cells following DMM treatment, and citrate levels were increased as well. The DMM-dependent increase in malate and citrate content was, however, removed after ME1 overexpression (Fig. 2, *C* and *D*).

Effect of ME1 on MSSIS and cytosolic Ca^{2+}. It has been hypothesized (27) that, in contrast to rat islets, the lack of ME1 activity in mouse islets may explain the absence of MSSIS in mouse islets. Contrary to this hypothesis, MSSIS was not

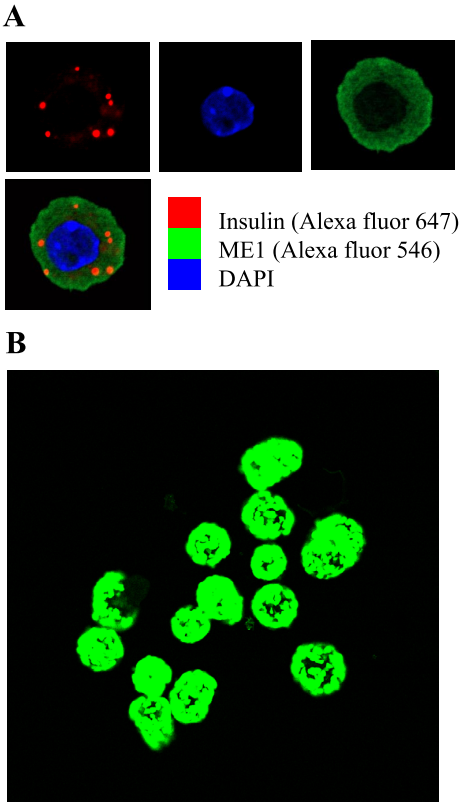

Fig. 1. Cytosolic malic enzyme (ME1) expression in a single mouse β-cell and an intact islet. *A*: intracellular localization of human ME1 (hME1) protein was determined using an anti-hME1 antibody and Alexa fluor 546. Insulin was detected using anti-insulin antibody and Alexa fluor 647. Nuclei were detected using 4′,6-diamidino-2-phenylindole (DAPI). *B*: a group of mouse islets infected with Ad-ME1-GFP. Strength of the green fluorescent protein (GFP) signal (excitation at 488/550 nm) was used to determine infection efficiency.

restored in whole mouse islets after ME1 expression (Fig. 3*A*). A group of islets infected with Ad-ME1-GFP is shown in Fig. 1*B* to demonstrate that infection with adenovirus was not limited to the outer cell layer of islets. In a parallel experiment, freshly isolated mouse islets were dispersed, yielding a population of single islet cells. After overnight culture in poly-D-lysine-coated culture vessels, single islet cells were infected with Ad-ME1-GFP. Although this approach ensured that >95% of cells were infected, it did not change the outcome: although 10 mM glucose stimulated secretion at 289 ± 32% of basal secretion, MS did not elicit secretion above the basal level (98 ± 16% of basal, where basal secretion was 18.4 ± 2.3 ng insulin·mg protein^{-1}·h^{-1}).

A rise in cytosolic Ca^{2+} accompanies insulin secretion and has been shown to occur during MS stimulation in rat islet cells (17). The inability of ME1-transduced mouse islet cells to respond to MS was further defined by determination of the Ca^{2+} response in single mouse islet cells. Since GFP was coexpressed in cells expressing ME1, the Ca^{2+} indicator Fura Fed (far red emission) was used to avoid cross-contamination with the GFP signal (14). In contrast to other Ca^{2+} indicators such as fluo 4, the intensity of Fura Red decreases on binding to Ca^{2+} (15). Thus an increase in the Ca^{2+} levels will be paralleled by a decrease in the Fura Red signal. Of 120 (ME1-overexpressing) and 134 (control) single β-cells, none responded to MS, whereas 77% and 79% of cells, respectively,

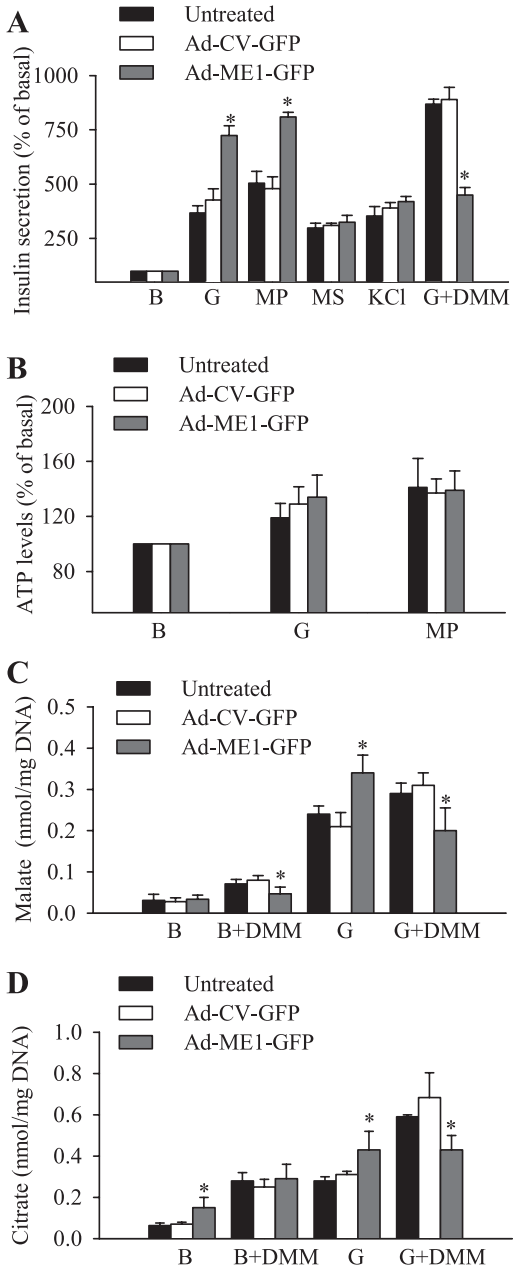

Fig. 2. Effect of ME1 overexpression on insulin secretion, ATP, and metabolite levels in INS-1 832/13 cells. INS-1 832/13 cells were left untreated or transduced with Ad-CV-GFP or Ad-ME1-GFP in the absence or presence of Ad-CytoLuc at 50 multiplicity of infection. *A*: after 2 h of preincubation in the presence of 2 mM glucose (G), insulin secretion in response to secretory fuels at 10 mM or KCl was measured in static incubation over a 30-min period. Basal secretion (B) at 2 mM glucose was 20.5 ± 2.2, 23.2 ± 3.1, and 22 ± 2.7 ng insulin·mg protein^{-1}·h^{-1} in untreated, Ad-CV-GFP-treated, and Ad-ME1-GFP-treated cells, respectively. Nonstimulatory 2 mM glucose was present during incubation with methyl pyruvate (MP), methyl succinate (MS), and KCl; stimulatory 10 mM glucose was present during incubation with dimethyl malate (DMM). Values are means ± SE from 5 independent experiments. *B*: ATP levels, measured in real time as relative light output, were determined in a population of ~0.5 × 10^6 live cells using the luciferin-luciferase reaction in response to 10 mM glucose and MP. Values are means ± SE from 4 independent measurements. *C* and *D*: malate and citrate levels were determined in mitochondrial fractions using tandem mass spectrometry (LC-MS/MS). *$P < 0.05$ vs. Ad-CV-GFP.

Table 2. *Effect of ME1 overexpression on ATP-to-ADP ratio and glucose oxidation in INS-1 832/13 cells*

	Untreated	Ad-CV-GFP	Ad-Me1-GFP
ATP-to-ADP ratio			
Basal	1.56±0.25	1.69±0.35	1.44±0.09
10 mM glucose	2.30±0.35	2.49±0.48	2.27±0.24
Glucose oxidation			
Basal	4.2±0.52	3.9±0.42	4.0±0.49
10 mM glucose	5.8±0.74	5.6±0.76	5.8±0.68

Values are means ± SE from 3 independent experiments. Glucose oxidation is expressed as nmol·mg protein^{-1}·90 min^{-1}. GFP, green fluorescent protein.

responded on subsequent stimulation with 10 mM glucose. (An example of such a response is presented in Fig. 4, *A* and *B*, respectively). These results suggest that there may be additional requirements for MSSIS besides ME1 activity or that MSSIS is unrelated to the ME1 activity. This notion is further supported by the fact that the mouse insulinoma cell line (MIN-6) possesses cytosolic $NADP^+$-dependent malate dehydrogenase activity, as demonstrated by MacDonald (27) and confirmed by us. However, these cells do not secrete insulin in response to MS, whereas they exhibit robust secretion in response to treatment with MP (Fig. 4*C*). To further assess the effect of MS on mouse islet metabolism, O_2 consumption was measured in mouse islets exposed to MS. Although rat islets demonstrated a sustained increase in O_2 consumption after MS application (Fig. 5*B*), mouse islets show only a transient increase (Fig. 5*A*). The lack of sustained increase in O_2 consumption in mouse islets was not changed by ME1 overexpression (Fig. 5*C*).

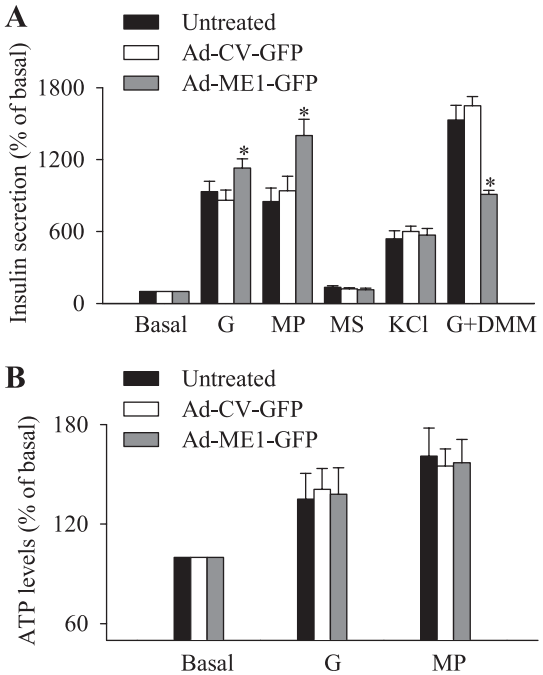

Fig. 3. Effect of ME1 overexpression on insulin secretion and ATP levels in mouse islets. Isolated mouse islets were left untreated or transduced with Ad-CV-GFP or Ad-ME1-GFP in the absence (secretion, *A*) or presence (ATP levels, *B*) of Ad-CytoLuc at 50 multiplicity of infection. *A*: after 2 h of preincubation in the presence of 4 mM glucose, insulin secretion was measured in response to secretory fuels at 10 mM or KCl in static incubation over a 30-min period. Basal secretion at 4 mM glucose was 3.2 ± 0.4, 3.7 ± 0.45, and 3.6 ± 0.5 ng insulin·10 islets^{-1}·h^{-1} in untreated, Ad-CV-GFP-treated, and Ad-ME1-GFP-treated islets, respectively. Nonstimulatory 4 mM glucose was present during incubation with MP, MS, and KCl. Stimulatory glucose (10 mM) was present during incubation with DMM. Values are means ± SE from 3–4 independent experiments. *B*: ATP production, measured as relative light output, was determined in a population of ~3.5 × 10^6 live islets cells (obtained by dispersion of whole islets) using the luciferin-luciferase reaction in response to stimulatory (10 mM) concentration of fuels. Values are means ± SE from 3 independent experiments. *$P < 0.05$ vs. Ad-CV-GFP.

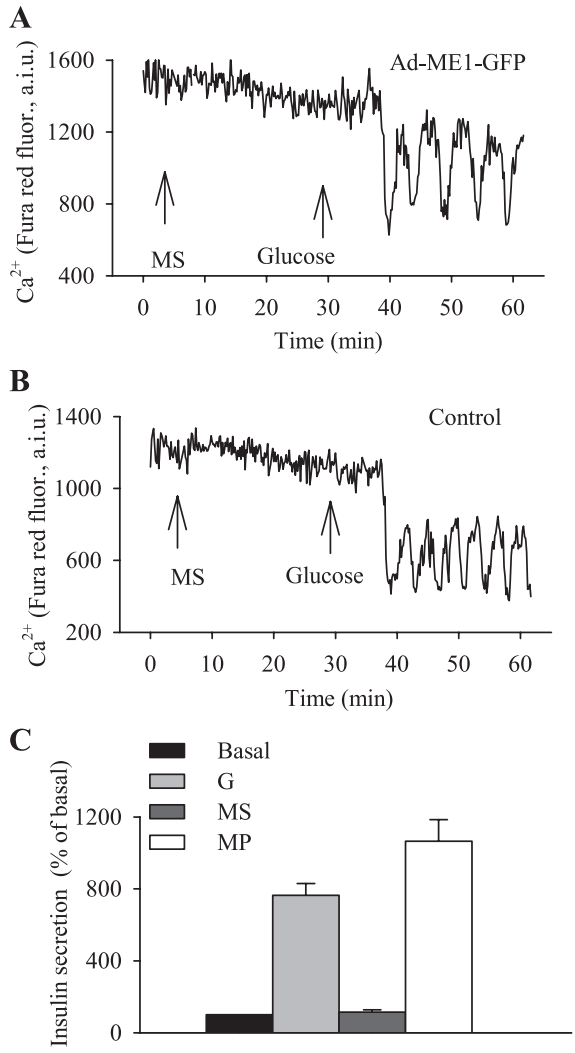

Fig. 4. MS-mediated metabolic response is not contingent on ME1 activity. *A* and *B*: a single mouse β-cell Ca^{2+} response in cells treated with Ad-ME1-GFP and in control cells. Addition of secretory fuels at 10 mM is indicated by arrows. Fura Red fluorescence is expressed as relative fluorescence units (F_1/F_0, where F_0 is mean baseline fluorescence). Note that Fura Red fluorescence intensity decreases upon Ca^{2+} binding (15). *C*: MIN-6 cells do not respond to MS, despite ME1 activity. After a 2-h preincubation in the presence of 2 mM glucose, MIN-6 cells were exposed to secretory fuels at 10 mM. Control cells were treated with 2 mM glucose (basal secretion). Insulin secretion was measured in static incubation over a 30-min period. Basal secretion was 56 ± 5.5 insulin·mg protein^{-1}·h^{-1}. $NADP^+$-dependent malate dehydrogenase activities were measured in the soluble protein fraction. Values are means ± SE from 4–5 independent experiments.

DISCUSSION

Evidence for and against the role of ME1 in GSIS has been previously reported (13, 39, 42). Mouse islets have been

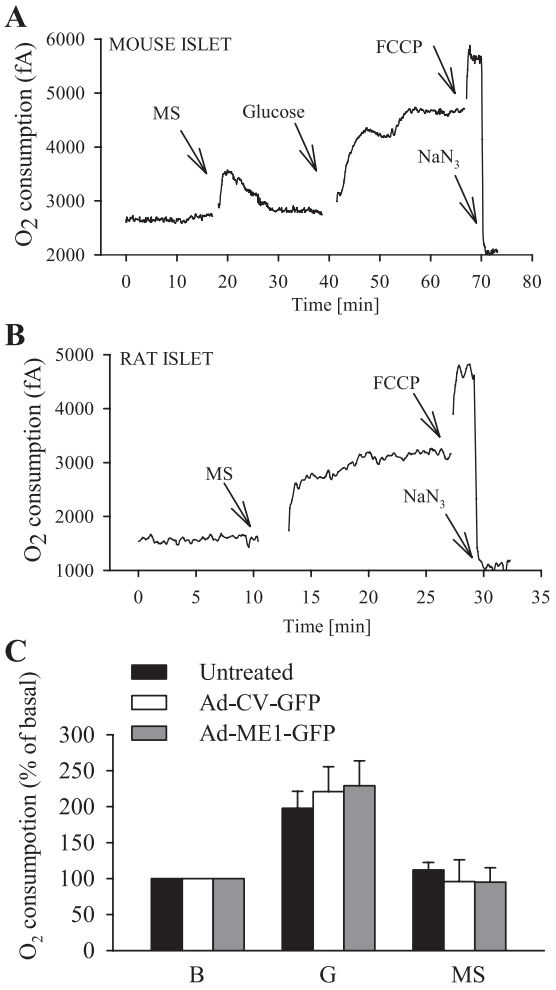

Fig. 5. Differential effect of MS on O_2 consumption in mouse and rat islets. *A*: MS does not stimulate a sustained increase in O_2 consumption in mouse islets. *B*: MS elicits a sustained increase in O_2 consumption in rat islets. Addition of fuels (10 mM) is indicated by arrows. Each trace is representative of 4–6 independent measurements. *C*: ME1 overexpression does not restore MS-mediated O_2 consumption in mouse islets. Values are means ± SE from 3 independent experiments.

reported to have no detectable ME1 activity (2, 17, 27); however, this view has been recently challenged by reports demonstrating the presence of Me1 mRNA (23) and enzymatic activity in mouse islets, which was suggested to be significantly correlated to the absence of DTT in the homogenization buffer (51). We have tested this hypothesis by preparing mouse islet extract with and without DTT. However, we did not detect ME1 activity under either condition (data not shown). It is possible that the strain of mouse we used (CD-1), in contrast to the C57BL/6 mouse used by Xu et al. (51), is responsible for these differences. Nevertheless, the level of ME1 activity has been found to be significantly lower in mouse than in rat islets (51), and ME1 activity was not measured in the earlier study (23). In addition, a variety of regulatory events can mediate translation of this enzyme (6). The consequential absence or low level of malate-pyruvate and pyruvate-citrate cycling pathways was hypothesized to explain the lack of MSSIS in mouse islets (27). If this hypothesis were correct, introduction of ME1 into mouse islets would enable operation of malate-pyruvate and pyruvate-citrate pathways, restore the secretory response of mouse islets to MS, and enhance GSIS. In addition, we tested the effect of ME1 overexpression on the potentiating effect of DMM on GSIS, proposed earlier to occur via activation of pyruvate cycling pathways (5).

ME1 overexpression increases GSIS and malate and citrate levels in INS-1 832/13 cells. ME1 overexpression increased GSIS in INS-1 832/13 cells and was paralleled by an increase in mitochondrial malate and citrate levels. This suggests that ME1 overexpression resulted in increased anaplerosis. An increase in citrate synthesis will require an increase in malate, but the mechanism by which malate is increased after ME1 overexpression is not clear. Pyruvate carboxylation to malate in islets is typically thought to occur via the enzyme pyruvate carboxylase (PC). It is possible that a side effect of ME1 overexpression is alteration of PC expression or activity, which would result in increased malate formation from pyruvate. However, ME1 is also capable of carboxylating pyruvate, as has been demonstrated in liver, muscle, and brain tissue (8, 50, 52). Furthermore, we have demonstrated that ME1 purified from the pancreatic cell line INS-1 832/13 is also capable of mediating this reaction. Whether the reaction catalyzed by ME1 will proceed toward malate formation (oxidative decarboxylation of pyruvate) or pyruvate formation (reductive carboxylation of malate) will be influenced by cytosolic levels and subcompartmentalization of its reactants and products, malate and pyruvate, as well as the NADPH-to-$NADP^+$ ratio and the concentration of CO_2. Under increased cytosolic pyruvate levels (e.g., glycolysis), we speculate that ME1 catalyzes the reaction that proceeds toward malate, rather than toward pyruvate, resulting in the elevated levels of malate found in cells overexpressing ME1. This would be further enhanced by the constitutively high NADPH-to-$NADP^+$ ratio (17) and the presence of CO_2 (7). Cytosolic malate, a product of this reaction, can enter the mitochondria and promote citrate synthesis and its export via the tricarboxylate carrier. Although we have demonstrated that ME1 overexpression increases malate levels, future studies are required to unambiguously demonstrate whether PC, ME1, or both are the principal mediators of enhanced malate and citrate formation in cells overexpressing ME1.

It is not clear how much cytosolic pyruvate, derived from glycolysis, can enter the mitochondria and how much can undergo oxidative carboxylation to form malate via ME1. Our view, however, is consistent with the notion that separate pyruvate pools (mitochondrial and extramitochodrial) exist within the β-cell (24). Furthermore, studies suggest that, even within the cytosol itself, a single metabolite can be distributed within more than one pool (3, 4). In hepatocytes, data supporting the existence of at least two separate cytosolic pyruvate pools, one associated with glycolysis and lactate (the glycolytic pool) and another with mitochondrial pyruvate, have been presented (38). A higher proportion of the glycolytic pyruvate pool available for carboxylation via ME1 in INS-1 832/13 cells than in mouse islets could explain why ME1 overexpression increased GSIS to a greater extent in INS-1 832/13 cells than in mouse islets, and studies are underway to address this issue.

DMM potentiates GSIS by stimulating malate entry into the mitochondria. The role of malate import into the mitochondria was explored in studies with the membrane-permeable malate analog DMM. If potentiation of GSIS by DMM requires ME1-dependent malate-pyruvate cycling, then DMM would not potentiate secretion in mouse islets, which lack ME1

enzymatic activity. Conversely, overexpression of ME1 would enhance the potentiating effect of DMM on GSIS. However, we observed that DMM potentiated GSIS in mouse islets to the same extent as it did in INS-1 832/13 cells and that this effect of DMM on GSIS was abolished by ME1 overexpression in both preparations. Accordingly, DMM-dependent increases in malate and citrate levels were abolished following ME1 overexpression. In addition, the level of ME1 activity adjusted by varying viral titer was inversely correlated to the DMM potentiation of GSIS in mouse islets (data not shown). Thus malate entry into the mitochondria seems to be an important step during DMM-mediated potentiation of GSIS.

The potentiating effect of DMM on GSIS is likely a consequence of maintaining a balance in charges and masses of mitochondrial intermediates. In mitochondria, acetyl-CoA and oxaloacetate (OAA), formed from decarboxylation and carboxylation of pyruvate, respectively, condense to form citrate. It is established that mitochondrial pyruvate carboxylation and decarboxylation occur in an ~4:6 ratio (22, 25). Thus malate, entering the mitochondria from the cytosol, will replenish the mitochondrial OAA pool and serve as a counterion to promote citrate or isocitrate export on the tricarboxylate carrier via electroneutral exchange of malate^{2-} for tricarboxylate^{2-} (37). Thus the addition of DMM can promote all pyruvate cycling pathways. Application of malate in the absence of glucose will not lead to tricarboxylate export, since acetyl-CoA will be depleted by condensation with OAA. Accordingly, application of DMM in the absence of stimulatory levels of glucose does not promote insulin secretion (data not shown).

When ME1 is overexpressed in INS-1 832/13 cells and introduced into mouse islets, exogenously applied malate (as DMM) will be converted to pyruvate, as the forward reaction of ME1 will be favored by abundance of this substrate. This will decrease the cytosolic malate pool available for entry to the mitochondria. Interestingly, although malate has been shown to accumulate inside the intact cells (46) and is transported out of isolated islet mitochondria (28), there is no report demonstrating malate export out of the mitochondria of intact cells under physiological levels of stimulatory glucose. However, citrate export out of the mitochondria in permeabilized cells has been demonstrated (9). Cytosolic citrate can undergo cleavage by citrate lyase to produce OAA and acetyl-CoA. Although evidence has been presented against the involvement of long-chain CoA (malonyl-CoA) (1, 36), short-chain acyl-CoAs have been recently implicated in insulin secretion (30, 31).

The activity of isocitrate dehydrogenase has been reported to be relatively high in mouse islets compared with rat and human islets (26), perhaps to compensate for the lack of a shuttle requiring ME1 activity. It is plausible that the transport of malate, derived from DMM, to the mouse islet mitochondria is balanced by export of isocitrate. Isocitrate can be converted to α-KG with generation of NADPH, and α-KG enters the mitochondria.

MSSIS and malic enzyme. MSSIS was not restored after introduction of ME1 in mouse islets, nor was MSSIS enhanced in INS-1 832/13 cells after ME1 overexpression. The original hypothesis linking MSSIS to the presence of ME1 activity (27) is based on the observation that malate is the main metabolite transported out of isolated mitochondria from rat and mouse islets in response to pyruvate and succinate (28). In the cytosol of rat β-cells, malate would be converted to pyruvate by the action of the cytosolic ME1 and pyruvate would reenter mitochondria (26), thus completing the cycle of the malate-pyruvate pathway. In the cytosol of mouse β-cells, exported malate would not be converted to pyruvate because of the absence or a low level of ME1 activity. Differences between our results and the above-described hypothesis (28) might be a result of different types of preparations. Isolated mitochondria, in contrast to intact cells, cannot account for factors that are likely to be important for transport, such as the metabolite concentration gradient between mitochondrial and cytosolic compartments (11, 45). It could be speculated, based on our results, that malate export out of the mitochondria in response to MS does not take place in intact β-cells, and our data demonstrating the

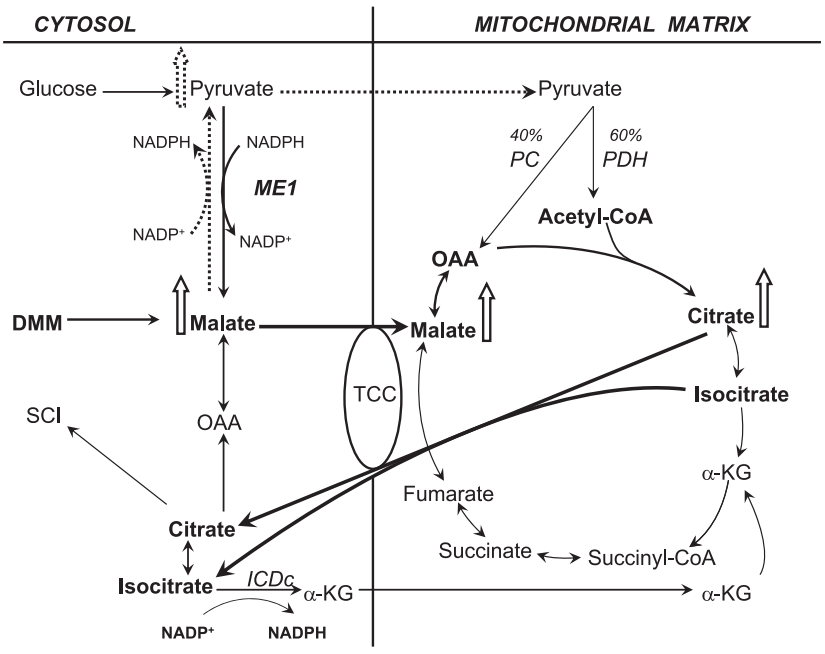

Fig. 6. DMM enhances insulin secretion: role of malate import into mitochondria. At initially high levels of cytosolic pyruvate (glycolysis) and low levels of cytosolic malate, the ME1-catalyzed reaction proceeds in the direction of malate formation and cytosolic malate enters mitochondria, resulting in increased output of citrate or isocitrate and enhanced insulin secretion. However, when the level of cytosolic malate becomes high (e.g., after DMM application), the ME1-dependent reaction functions in reverse, favoring pyruvate formation (dotted line), resulting in decreased citrate/isocitrate output and insulin secretion. Under the second condition, increased ME1 activity (ME1 overexpression) compared with cells with lower endogeneous (INS-1 832/13) or low or absent (mouse islets) ME-1 activity facilitates removal of cytosolic malate and removes DMM potentiation of glucose-stimulated insulin secretion (GSIS) via decreased citrate/isocitrate output. OAA, oxaloacetate; TCC, tricarboxylate carrier; ICDc, cytosolic isocitrate dehydrogenase; α-KG, α-ketoglutarate; PC, pyruvate carboxylase; PDH, pyruvate dehydrogenase; SCI, secretory coupling intermediates.

lack of enhancement of MSSIS in INS-1 832/13 cells support this notion. However, solely on the basis of the inability of ME1 activity to restore MSSIS in the mouse β-cells, the possibility that malate is exported from the mitochondria in exchange for succinate on the dicarboxylate carrier cannot be completely ruled out (Fig. 6) (10). Differences in the activities of mitochondrial metabolite carriers between mouse and rat β-cells might also be responsible for the failure of ME1 to restore MSSIS in mouse. The absence or a low activity of the specific dicarboxylate carrier can serve as an alternative explanation for the failure of MS to trigger insulin secretion in mouse islets as follows. Insufficient malate transport out of mitochondria would halt succinate import and eventually cause cessation of the insulin secretion response. Although MS is an inefficient secretagogue in mouse islets, it does trigger a transient increase in the ATP-to-ADP ratio (17) and O_2 consumption (Fig. 5) in these islets. In addition, MS fails to stimulate insulin secretion in mouse insulinoma MIN-6 cells, which possess high levels of ME1 activity (Fig. 4*C*). Although the important role of mitochondrial carriers in GSIS has just started to be recognized (21), there is still a lack of knowledge about the relative importance of individual carriers for the mechanism of action of a particular fuel secretagogue in the β-cell, and studies are underway to address these issues.

In summary, we have demonstrated that overexpression of ME1 augments insulin secretion in INS-1 832/13 cells and that the underlying mechanism likely involves increased citrate synthesis, although the exact mechanism is not clear. The fact that ME1 overexpression did not significantly affect GSIS in isolated mouse islets is consistent with the recent report demonstrating no effect of ME1 silencing on GSIS in primary rat islets (42). We speculate that differences in size and compartmentalization of the metabolite pools within the cell (in this case, the cytosolic pyruvate pool, which is available for carboxylation via the reverse reaction of ME1) between clonal insulinoma cells and primary islets might underlie the failure of ME1 expression to greatly enhance GSIS in mouse islets. Transport of malate to the mitochondria likely promotes the efflux of citrate or isocitrate and activation of the corresponding cycling pathway, resulting in production of NADPH. Although our view does not support the role of the pyruvate-malate cycling pathway in GSIS and MSSIS, it is consistent with key features demonstrated to play a role in insulin secretion, including pyruvate carboxylation, tricarboxylate efflux, and NADPH generation. Thus these data further the current understanding of metabolic changes underlying insulin secretion.

ACKNOWLEDGMENTS

We thank Prof. M. Meow for helpful comments and support in the manuscript preparation.

J. P. Gray is a professor at the US Coast Guard Academy. The views here are his own and not necessarily those of the Academy or other branches of the US Government.

GRANTS

This work was supported by American Diabetes Association Grant 7-08-JF-18 (E. Heart), Division of Research Resources Grant P41-RR-001395 (P. J. S. Smith), and National Institute of Diabetes and Digestive and Kidney Diseases Grants DK-063984 (P. J. S. Smith) and DK-071071 (G. W. Cline).

REFERENCES

1. **Antinozzi PA, Segall L, Prentki M, McGarry JD, Newgard CB.** Molecular or pharmacologic perturbation of the link between glucose and lipid metabolism is without effect on glucose-stimulated insulin secretion. A re-evaluation of the long-chain acyl-CoA hypothesis. *J Biol Chem* 273: 16146–16154, 1998.
2. **Ashcroft SJ, Randle PJ.** Enzymes of glucose metabolism in normal mouse pancreatic islets. *Biochem J* 119: 5–15, 1970.
3. **Berry MN.** The function of energy-dependent redox reactions in cell metabolism. *FEBS Lett* 117 *Suppl*: K106–K120, 1980.
4. **Berry MN, Fanning DC, Grivell AR, Lewis SJ, Farrington CJ, Wallace PG.** Evidence for several separate functional pools of NAD(H) within the cytoplasmic compartment of the hepatocyte. *Biochem Soc Trans* 8: 570, 1980.
5. **Boucher A, Lu D, Burgess SC, Telemaque-Potts S, Jensen MV, Mulder H, Wang MY, Unger RH, Sherry AD, Newgard CB.** Biochemical mechanism of lipid-induced impairment of glucose-stimulated insulin secretion and reversal with a malate analogue. *J Biol Chem* 279: 27263–27271, 2004.
6. **Brown ML, Wise LS, Rubin CS.** The molecular basis for a cytosolic malic enzyme null mutation. Malic enzyme mRNA from MOD-1 null mice contains an internal in-frame duplication that extends the coding sequence by 522 nucleotides. *J Biol Chem* 263: 4494–4499, 1988.
7. **Buanes T, Grotmol T, Landsverk T, Nafstad P, Raeder MG.** Effects of arterial pH and carbon dioxide on pancreatic exocrine H^+/HCO_3^- secretion and secretin-dependent translocation of cytoplasmic vesicles in pancreatic duct cells. *Acta Physiol Scand* 133: 1–9, 1988.
8. **Bukato G, Kochan Z, Swierczynski J.** Purification and properties of cytosolic and mitochondrial malic enzyme isolated from human brain. *Int J Biochem Cell Biol* 27: 47–54, 1995.
9. **Farfari S, Schultz V, Corkey BE, Prentki M.** Glucose-regulated anaplerosis and cataplerosis in pancreatic β-cells. Possible implication of a pyruvate/citrate shuttle in insulin secretion. *Diabetes* 49: 718–726, 2000.
10. **Fiermonte G, Palmieri L, Dolce V, Lasorsa FM, Palmieri F, Runswick MJ, Walker JE.** The sequence, bacterial expression, and functional reconstitution of the rat mitochondrial dicarboxylate transporter cloned via distant homologs in yeast and *Caenorhabditis elegans*. *J Biol Chem* 273: 24754–24759, 1998.
11. **Frezza C, Cipolat S, Scorrano L.** Organelle isolation: functional mitochondria from mouse liver, muscle and cultured fibroblasts. *Nat Protoc* 2: 287–295, 2007.
12. **Gray JP, Heck DE, Mishin V, Smith PJ, Hong JY, Thiruchelvam M, Cory-Slechta DA, Laskin DL, Laskin JD.** Paraquat increases cyanide-insensitive respiration in murine lung epithelial cells by activating an NAD(P)H:paraquat oxidoreductase: identification of the enzyme as thioredoxin reductase. *J Biol Chem* 282: 7939–7949, 2007.
13. **Guay C, Madiraju SR, Aumais A, Joly E, Prentki M.** A role for ATP-citrate lyase, malic enzyme, and pyruvate/citrate cycling in glucose-induced insulin secretion. *J Biol Chem* 282: 35657–35665, 2007.
14. **Hara M, Wang X, Kawamura T, Bindokas VP, Dizon RF, Alcoser SY, Magnuson MA, Bell GI.** Transgenic mice with green fluorescent protein-labeled pancreatic β-cells. *Am J Physiol Endocrinol Metab* 284: E177–E183, 2003.
15. **Haugland R.** In: *Handbook of Fluorescent Probes and Research Chemicals*. Eugene, OR: Molecular Probes, 2002, sect. 20.4.
16. **Heart E, Smith PJS.** Rhythm of the β-cell oscillator is not governed by a single regulator: multiple systems contribute to oscillatory behavior. *Am J Physiol Endocrinol Metab* 292: E1295–E1300, 2007.
17. **Heart E, Yaney GC, Corkey RF, Schultz V, Luc E, Liu L, Deeney JT, Shirihai O, Tornheim K, Smith PJS, Corkey BE.** Ca^{2+}, NAD(P)H and membrane potential changes in pancreatic beta-cells by methyl succinate: comparison with glucose. *Biochem J* 403: 197–205, 2007.
18. **Henquin J.** Triggering and amplifying pathways of regulation of insulin secretion by glucose. *Diabetes* 49: 1751–1760, 2000.
19. **Hohmeier HE, Mulder H, Chen G, Henkel-Rieger R, Prentki M, Newgard CB.** Isolation of INS-1-derived cell lines with robust ATP-sensitive K^+ channel-dependent and -independent glucose-stimulated insulin secretion. *Diabetes* 49: 424–430, 2000.
20. **Ivarsson R, Quintens R, Dejonghr S, Tsukamoto K, Veld P, Renstrom E, Schuit FC.** Redox control of exocytosis. Regulatory role of NADPH, thioredoxin, and glutaredoxin. *Diabetes* 54: 2132–2142, 2005.
21. **Joseph JW, Jensen MV, Ilkayeva O, Palmieri F, Alarcon C, Rhodes CJ, Newgard CB.** The mitochondrial citrate/isocitrate carrier plays a

regulatory role in glucose-stimulated insulin secretion. *J Biol Chem* 281: 35624–35632, 2006.
22. **Khan A, Ling ZC, Landau BR.** Quantifying the carboxylation of pyruvate in pancreatic islets. *J Biol Chem* 271: 2539–2542, 1996.
23. **Li C, Nissim I, Chen P, Buettger C, Najafi H, Daikhin Y, Nissim I, Collins HW, Yudkoff M, Stanley CA, Matschinsky FM.** Elimination of K_{ATP} channels in mouse islets results in elevated [U-^{13}C]glucose metabolism, glutaminolysis, and pyruvate cycling but a decreased γ-aminobutyric acid shunt. *J Biol Chem* 283: 17238–17249, 2008.
24. **Lu D, Mulder H, Zhao P, Burgess SC, Jensen MV, Kamzolova S, Newgard CB, Sherry AD.** ^{13}C NMR isotopomer analysis reveals a connection between pyruvate cycling and glucose-stimulated insulin secretion (GSIS). *Proc Natl Acad Sci USA* 99: 2708–2713, 2002.
25. **MacDonald MJ.** Glucose enters mitochondrial metabolism via both carboxylation and decarboxylation of pyruvate in pancreatic islets. *Metabolism* 42: 1229–1231, 1993.
26. **MacDonald MJ.** Feasibility of a mitochondrial pyruvate malate shuttle in pancreatic islets. Further implication of cytosolic NADPH in insulin secretion. *J Biol Chem* 270: 20051–20058, 1995.
27. **MacDonald MJ.** Differences between mouse and rat pancreatic islets: succinate responsiveness, malic enzyme, and anaplerosis. *Am J Physiol Endocrinol Metab* 283: E302–E310, 2002.
28. **MacDonald MJ.** Export of metabolites from pancreatic islet mitochondria as a mean to study anaplerosis in insulin secretion. *Metabolism* 52: 993–998, 2003.
29. **MacDonald MJ, Fahien LA.** Glutamate is not a messenger in insulin secretion. *J Biol Chem* 275: 34025–34027, 2000.
30. **MacDonald MJ, Longacre MJ, Stoker SW, Brown LJ, Hasan NM, Kendrick MA.** Acetoacetate and β-hydroxybutyrate in combination with other metabolites release insulin from INS-1 cells and provide clues about pathways in insulin secretion. *Am J Physiol Cell Physiol* 294: C442–C450, 2008.
31. **MacDonald MJ, Smith AD 3rd, Hasan NM, Sabat G, Fahien LA.** Feasibility of pathways for transfer of acyl groups from mitochondria to the cytosol to form short chain acyl-CoAs in the pancreatic beta cell. *J Biol Chem* 282: 30596–30606, 2007.
32. **Maechler P, Wollheim CB.** Mitochondrial glutamate acts as a messenger in glucose-induced insulin exocytosis. *Nature* 402: 685–689, 1999.
33. **McElroy WD.** The energy source for bioluminescence in an isolated system. *Proc Natl Acad Sci USA* 33: 342–345, 1947.
34. **Misler S, Barnett G, Gilis KD, Pressel DM.** Electrophysiology of stimulus-secretion coupling in human β-cells. *Diabetes* 41: 1221–1228, 1992.
35. **Miyazaki J, Araki K, Yamato E, Ikegami H, Asano T, Shibasaki Y, Oka Y, Yamamura K.** Establishment of a pancreatic beta cell line that retains glucose-inducible insulin secretion: special reference to expression of glucose transporter isoforms. *Endocrinology* 127: 126–132, 1990.
36. **Mulder H, Lu D, Finley J, An J, Cohen J, Antinozzi PA, McGarry JD, Newgard CB.** Overexpression of a modified human malonyl-CoA decarboxylase blocks the glucose-induced increase in malonyl-CoA level but has no impact on insulin secretion in INS-1-derived (832/13) beta-cells. *J Biol Chem* 276: 6479–6484, 2001.
37. **Palmieri F.** The mitochondrial transporter family (SLC25): physiological and pathological implications. *Pflügers Arch* 447: 689–709, 2004.
38. **Peuhkurinen KJ, Hiltunen JK, Hassinen IE.** Metabolic compartmentation of pyruvate in the isolated perfused rat heart. *Biochem J* 210: 193–198, 1983.
39. **Pongratz RL, Kibbey RG, Shulman GI, Cline GW.** Cytosolic and mitochondrial malic enzyme isoforms differentially control insulin secretion. *J Biol Chem* 282: 200–207, 2007.
40. **Prentki M, Vischer S, Glennon MC, Regazzi R, Deeney JT, Corkey BE.** Malonyl-CoA and long chain acyl-CoA esters as metabolic coupling factors in nutrient-induced insulin secretion. *J Biol Chem* 267: 5802–5810, 1992.
41. **Ronnebaum SM, Ilkayeva O, Burgess SC, Joseph JW, Lu D, Stevens RD, Becker TC, Sherry AD, Newgard CB, Jensen MV.** A pyruvate cycling pathway involving cytosolic NADP-dependent isocitrate dehydrogenase regulates glucose-stimulated insulin secretion. *J Biol Chem* 281: 30593–30602, 2006.
42. **Ronnebaum SM, Jensen MV, Hohmeier HE, Burgess SC, Zhou YP, Qian S, Macneil D, Howard A, Thornberry N, Ilkayeva O, Lu D, Sherry AD, Newgard CB.** Silencing of cytosolic or mitochondrial isoforms of malic enzyme has no effect on glucose-stimulated insulin secretion from rodent islets. *J Biol Chem* 283: 28909–28917, 2008.
45. **Salnikov V, Lukyanenko YO, Frederick CA, Lederer WJ, Lukyanenko V.** Probing the outer mitochondrial membrane in cardiac mitochondria with nanoparticles. *Biophys J* 92: 1058–1071, 2007.
46. **Schuit F, De VA, Farfari S, Moens K, Pipeleers D, Brun T, Prentki M.** Metabolic fate of glucose in purified islet cells. Glucose-regulated anaplerosis in beta cells. *J Biol Chem* 272: 18572–18579, 1997.
47. **Skorkowski EF, Storey KB.** Affinity chromatography on 2′,5′-ADP-Sepharose 4B for purification of malic enzyme from crustacean muscle. *J Chromatogr* 389: 427–432, 1987.
48. **Smith PJS, Sanger RH, Messerli MA.** Electrochemical methods for neuroscience. In: *Principles, Development and Applications of Self-Referencing Electrochemical Microelectrodes to the Determination of Fluxes at Cell Membranes*. Boca Raton, FL: CRC, 2007, p. 373–405.
49. **Swierczynski J.** Purification and some properties of extramitochondrial malic enzyme from rat skeletal muscle. *Biochim Biophys Acta* 616: 10–21, 1980.
50. **Swierczynski J, Aleksandrowicz Z, Zelewski L.** Carboxylation of pyruvate via extramitochondrial malic enzyme in rat skeletal muscle. *Acta Biochim Pol* 33: 47–54, 1986.
51. **Xu J, Han J, Long YS, Lock J, Weir GC, Epstein PN, Liu YQ.** Malic enzyme is present in mouse islets and modulates insulin secretion. *Diabetologia* 51: 2281–2289, 2008.
52. **Zelewski M, Swierczynski J.** Malic enzyme in human liver. Intracellular distribution, purification and properties of cytosolic isozyme. *Eur J Biochem* 201: 339–345, 1991.